ChemComm

COMMUNICATION

View Article Online
View Journal | View Issue

Cite this: *Chem. Commun.*, 2025, **61**, 568

Received 24th September 2024,
Accepted 4th December 2024

DOI: 10.1039/d4cc04956j

rsc.li/chemcomm

Constructing LiF-rich cathode electrolyte interphase to enhance the cyclic stability of lithium-rich manganese-based oxide cathode†

Yang Yang,[ab] Yajun Zhao,[a] Junjie Song,[ab] Xiqian Yu *[ab] and Hong Li *[ab]

Lithium-rich manganese-based oxide (LRMO) materials hold great potential for high-energy-density lithium-ion batteries (LIBs) but suffer from severe voltage decay and capacity fading. Herein, we report the *in situ* construction of LiF-rich solid electrolyte interphase on LRMO through a straightforward ball-milling and electrochemical approach, which exhibits remarkable structural stability and enhanced electrochemical performance.

To realize the goal of peak carbon dioxide emissions and global carbon neutrality, the development of LIBs with high-energy-density is highly important, as they represent one of the most effective energy storage solutions for grid applications and green-power transportation.[1] While traditional cathode materials such as $LiFePO_4$ and $LiMn_2O_4$ have been commercialized for decades, their constrained theoretical capacity and low operating voltage present significant challenges for the achievement of high-energy density LIBs.[2,3] Recently, LRMO materials have emerged as promising high-capacity cathodes due to their ability to facilitate multiple electron reactions stemming from both cationic and anionic redox processes.[4] These materials can achieve high capacities of up to 250 mA h g^{-1} and high energy densities reaching 1000 W h kg^{-1}, highlighting their potential for applications in next-generation high-energy-density LIBs.[5–8]

The instability of lattice oxygen in LRMO at high charging voltages poses a significant challenge to their practical applications. When the voltage is charged to 4.5 V, the lattice oxygen participates in a redox reaction, leading to irreversible oxygen loss that progressively propagates from the surface into the interior of the material. This process underlies the electrochemical degradation of the LRMO cathode.[9–11] Moreover, as the voltage is elevated to higher levels (~4.8 V), oxygen release at surface regions is remarkably aggravated, resulting in severe chain reactions, such as irreversible phase transformation and electrolyte decomposition.[12–14] Given that the cathode surface serves as the interface for oxygen evolution, ensuring its stability against oxygen release is crucial for improving the cycling stability of LRMOs.[15,16]

The coating is one of the most effective strategies for enhancing the surface stability of the LRMOs.[17] Specifically, the construction of a LiF-rich protective interface on these materials can greatly improve their electrochemical performance at high voltages. This is because the interface film exhibits both chemical and electrochemical stability, effectively preventing oxidized lattice oxygen anions from interacting with electrolytes.[18–22] The use of fluorinated electrolytes has been shown to facilitate the formation of a LiF-rich cathode electrolyte interphase (CEI).[23] However, the incorporation of these electrolytes may sometimes lead to a reduction in conductivity, which presents additional challenges for performance. Furthermore, their high cost and environmental impact pose concerns for commercial applications.[24] Another alternative way involves the application of fluorinated substances as a coating. For instance, Liu *et al.* proposed a sol–gel method followed by calcination treatment to fabricate F-doped carbon-modified $Li_{1.2}Mn_{0.54}Ni_{0.13}Co_{0.13}O_2$ with higher discharged capacity and enhanced capacity retention.[25] However, these methods either involve high costs and environmental hazards or require a tedious fabrication process, which is relatively unfavourable for large-scale production. Consequently, it is crucial to develop a cost-effective and systematic strategy for achieving a uniform LiF-rich CEI coating on the LRMOs to facilitate their further applications.[26]

Herein, we present an *in situ* method for constructing a LiF-rich CEI on $Li_{1.2}Mn_{0.54}Ni_{0.13}Co_{0.13}O_2$ cathode particles through a facile ball-milling process with fluorinated carbon (CF) followed by an electrochemical conversion process ($CF_x + xLi \rightarrow C + xLiF$). Benefiting from the high chemical stability of LiF and nano-sized carbon with enhanced conductivity, the

[a] *Institute of Physics, Chinese Academy of Sciences, Beijing, 100190, China. E-mail: xyu@iphy.ac.cn, hli@iphy.ac.cn*
[b] *Center of Materials Science and Optoelectronics Engineering, University of Chinese Academy of Sciences, Beijing, 100049, China*

† Electronic supplementary information (ESI) available. See DOI: https://doi.org/10.1039/d4cc04956j

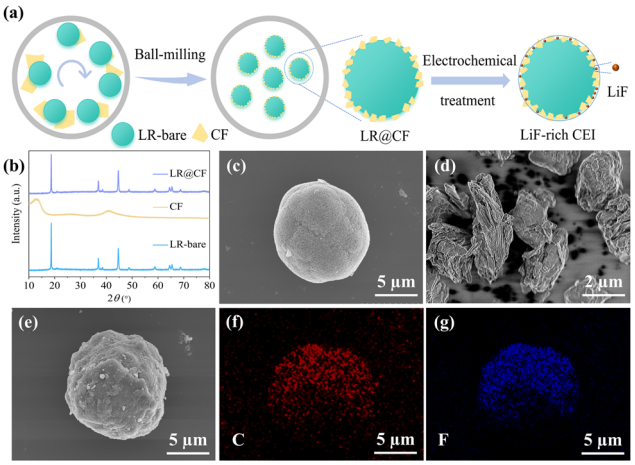

Fig. 1 (a) Schematic diagram of the process of coating CF on LR-bare surface and the formation of LiF-rich CEI. (b) XRD patterns of LR-bare, CF and LR@CF. SEM images of (c) LR-bare, (d) CF and (e) LR@CF. The EDS mapping spectrum of (f) C and (g) F for LR@CF.

obtained 3 wt% CF-coated LRMO (designated as LR@CF) demonstrates remarkable electrochemical performance. It achieved a high specific discharge capacity of 305.5 mA h g^{-1} at 0.1C, along with an improved capacity retention of 94.07% after 100 cycles at 1C. This work elucidates that the *in situ* formation of a LiF-rich protective interface through a simple ball-milling strategy is an effective approach to enhance the electrochemical performance of the LRMO cathode.

The process of *in situ* fabrication of carbon and LiF-rich CEI layer on the LRMO cathode particle surface is illustrated in Fig. 1a. By controlling the treatment time and rotation speed of high-energy ball milling, the micro-sized CF the micro-sized CF is fragmented into nanoscale particles and densely coated on the surface of LRMO particles. Subsequently, the obtained LR@CF is treated by electrochemical cycling. During the first discharging process, the CF can be converted to C and LiF, thereby facilitating the *in situ* production of carbon and LiF-rich CEI film on the surface of the LRMO particles.

To investigate the structural and morphologic characteristics of the synthesized LR@CF composite, powder X-ray diffraction (XRD) and scanning electron microscope (SEM) analyses were conducted. As shown in Fig. 1b, XRD patterns of CF, untreated LRMO (LR-bare), and LR@CF composite were collected respectively. The CF displays characteristic (0 0 1) and (1 0 0) crystal planes at approximately 12.8° and 41°.[27] For LR-bare, it exhibits typical diffraction peaks around 19.5°–22.5°, showing the typical Li_2MnO_3 phase with α-$NaFeO_2$ structure.[28] After ball milling treatment, LR@CF retains identical diffraction peaks as LR-bare without significant evidence of CF presence, suggesting that the micro-sized CF particles have been fragmented and coated on the surface of LRMO particles. The morphology evolution of LR@CF during milling treatment is displayed in Fig. 1c and e. The LR-bare exhibits a secondary spherical particle formed by the agglomeration of primary particles, with a size range from 5 μm to 15 μm. For CF, it processes an irregular and layered shape with a particle size of 2–6 μm (Fig. 1d). After the mixing of CF and LR-bare by ball milling, a dense coating of nano-size CF on the LR-bare surface can be observed. Some particles with small size on the surface of LR@CF are obvious (Fig. 1e and Fig. S1, ESI†), which is ascribed to CF particles with reduced size from micro-level to nano-level during ball milling treatment. Moreover, as shown in Fig. 1f and g, the energy dispersive spectroscope (EDS) mapping results reveal that both C and F elements are evenly distributed on the surface of the spherical particles of LR (Fig. S2, ESI†), confirming the successful coating of CF on the surface of the LR-bare particles.

The influence of varying CF coating contents on the electrochemical performance of LR@CF was further investigated. Fig. 2a shows the initial charge and discharge curves of bare LR with CF coating content of 1 wt% (LRCF1), 3 wt% (LRCF3), and 5 wt% (LRCF5) respectively. At a current density of 0.1C (1C = 250 mA h g^{-1}) in the voltage range of 2.0–4.8 V, the LR-bare, LRCF1, LRCF3, and LRCF5 exhibit specific charging capacities of 331.5, 317.8, 324.5, and 298.8 mA h g^{-1} respectively. Their corresponding discharging capacities are recorded as 293.3, 299.1, 305.5 and 298.8 mA h g^{-1} with initial coulombic efficiencies (ICE) of 88.48%, 94.11%, 94.15%, and 100%. It is evident that as the amount of CF coating increases, the charging capacity progressively decreases. Noteworthy, it is generally considered that the oxidation of electrolytes contributes to notable additional capacity when the charging voltage is above 4.6 V.[15] Thus, the reduced charging capacity observed in LRCF1, LRCF3, and LRCF5 indicates a decrease in side reactions from electrolytes due to the presence of CF. During the first discharge process, CF can provide capacity when the battery is discharged below 2.5 V, leading to the increased specific discharging capacities and the ICEs for the CF-modified LRMOs. However, the formation of reluctant LiF may occur due to an excessive amount of CF coating, which can cause higher polarization and thus lead to a reduction in capacity. Based on the analysis of electrochemical performance,

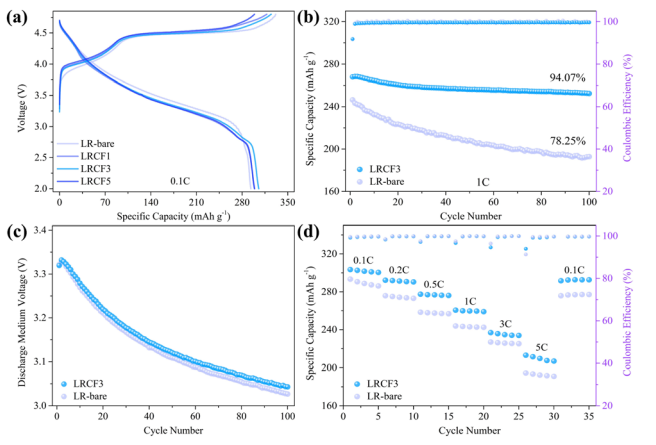

Fig. 2 (a) Initial charge–discharge curves of LR-bare and LR-bare coated with different mass of CF. (b) Comparison of cycle performance and (c) voltage decay at 1C between LR-bare and LRCF3. (d) Rate performance of LR-bare and LRCF3.

LRCF3 demonstrates superior electrochemical performance compared to other samples. Therefore, LRCF3 is selected as the optimal cathode for further investigation.

In the voltage range of 2.0–4.8 V at 1C, the LRCF3 exhibits a specific discharging capacity of 267.9 mA h g^{-1}, which represents an increase of 8.7% compared to LR-bare (246.4 mA h g^{-1}). After 100 cycles, the LRCF3 maintains superior capacity retention at 94.07%, in contrast to LR-bare's retention of 78.25% (Fig. 2b). The capacity fading of the two samples is more clearly demonstrated on the charge–discharge curves after 100 cycles (Fig. S3, ESI†). Moreover, the LRCF3 shows alleviated voltage decay during the long cycle process (Fig. 2c), and the single-cycle voltage decay has been reduced from 2.95 mV (LR-bare) to 2.76 mV. It implies that the coating layer inhibits the migration of transition metal (TM) induced by oxygen release, thereby effectively mitigating voltage decay and ensuring long cycling life of LRMO. Notably, the coating strategy can effectively mitigate, but not eliminate, voltage decay in LRMO, which may be attributed to the mechanical fatigue of the coating layer induced by electrochemical cycling. To further alleviate voltage decay, additional strategies should be considered, such as electrolyte design, particularly the development of highly stable solid-state electrolytes in the future.[15] The rate performance of LR-bare and LRCF3 are shown in Fig. 2d. For LR-bare, it exhibits specific discharging capacities of 293.3, 275.8, 258.4, 243.9, 227.0, and 194.6 mA h g^{-1} at 0.1C, 0.2C, 0.5C, 1C, 3C, and 5C, respectively. In contrast, the corresponding capacities increase to 303.4, 292.2, 277.4, 260.6, 236.9, and 213.1 mA h g^{-1} for LRCF3. It suggests that the rate performance of LR-bare can be improved by coating adequately with CF. Moreover, after the current density was recovered back to 0.1C, the LRCF3 still delivered a higher discharging capacity of 291.6 mA h g^{-1} compared to that of LR-bare (275.8 mA h g^{-1}). This indicates that the surface of the LRMO can sustain low resistance over prolonged cycling following the application of CF coating. Compared with other reported LRMO materials, the high electrochemical performances assure the LRCF3 cathode with high competitiveness (Table S1, ESI†). Ah-level full pouch-cells were further prepared with SiC as anode and LR-bare or LRCF3 as the cathode. As shown in Fig. S4a (ESI†), during the formation stage, the full pouch-cell using LRCF3 as the cathode exhibits higher charge/discharge capacity (1.31/0.99 A h) and coulombic efficiency (75.94%) than that of LR-bare (0.99/0.67 A h, 67.07%). Moreover, after 50 cycles at 0.5C, the LRCF3 still shows higher capacity retentions (85.72%) than that of LR-bare (4.18%) (Fig. S4b, ESI†). These results suggest that the modification strategy proposed in this work has great potential in large-scale application of LRMO with high electrochemical performance.

To further explore the working mechanisms for the electrochemical enhancement of LR@CF after CF coating, the electrochemical impedance spectroscopy (EIS) and X-ray photoelectron spectroscopy (XPS) experiments were performed on the LR-bare and LRCF3 samples after the first charge and discharge processes. As shown in Fig. 3a, EIS curves for both samples are fitted based on the equivalent circuit. Among them, the LRCF3

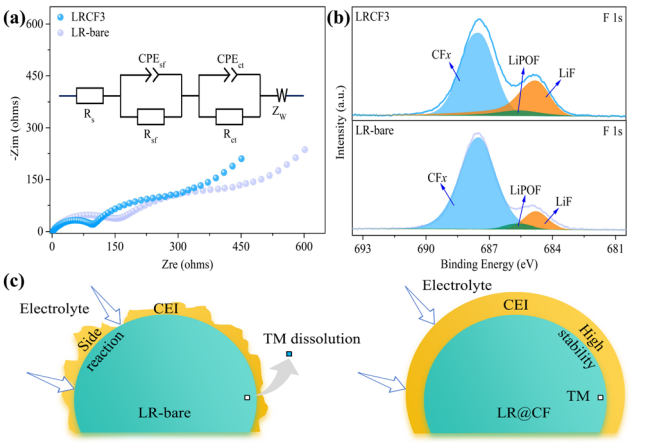

Fig. 3 (a) Impedance spectra and corresponding equivalent circuits of LR-bare and LRCF3 after the first discharge. (b) F 1s XPS spectra of LR-bare and LRCF3 after the initial discharge. (c) Schematic diagram of the mechanism by which CF coating improves LR performance.

exhibits a significantly smaller semicircle diameter than that of LR-bare at the middle-frequency region, suggesting that LRCF3 has a lower charge transfer resistance (R_{ct}) due to the existence of the electrochemically formed carbon in the coating layer.[29–32] Further, as shown in Table S2 (ESI†), both ohmic resistance (R_s) and surface film resistance (R_{sf}) for LRCF3 exhibit smaller values of 2.57 Ω and 109.1 Ω compared to that of LR-bare sample (3.13 Ω and 115.9 Ω). It reveals that the resultant carbon effectively enhances the conductivity of LRMO during the process of cycling, which indicates the improved rate performance of LRCF3.

XPS was conducted to investigate the surface chemical component of cycled LR-bare and LRCF3 cathode. As shown in Fig. 3b, in the F 1s XPS spectrum of LR-bare, characteristic peaks are observed at 685.8, 686.9, and 688.5 eV, which correspond to LiF, LiPOF, and CF_x, respectively.[18,33] The generated LiPOF can be attributed to the decomposition of $LiPF_6$ and the CF_x signal can be assigned to PVDF. Thus, it suggests that the CEI film on the LR-bare surface mainly consists of organic species and inorganic compounds (*i.e.* LiF). After the surface decoration, the XPS spectrum of the cycled LRCF3 cathode reveals a characteristic peak of LiF with enhanced intensity. This observation indicates a great increase in inorganic F-species, such as LiF, within the CEI, suggesting that CF plays a role in turning organic and inorganic species contents into CEI components. Furthermore, the intensity of LiPOF shows a slight decrease, implying that electrolyte decomposition is effectively inhibited due to the CF coating. This coating prevents direct contact between the cathode and electrolyte, thereby suppressing side reactions on the cathode surface during battery cycling. The C 1s spectrum also presented more prominent variations relevant to the surface components modified by CF. Given that it was merely the first charge–discharge cycle, the peak positions and intensities of elements including Ni, Co, and Mn did not change substantially (Fig. S5, ESI†).[25] These findings suggest that the introduction of CF provides an

adequate source of F to form a densely coated LiF-rich inorganic CEI on the LR-bare surface. This CEI can enhance the oxidation stability of LR@CF under high voltage and suppress the voltage decay caused by the migration of TM due to oxygen release, and also mitigate continuous side reactions between electrolyte and LRMO bulk. In addition, the electrochemically formed carbon endows LR@CF with high conductivity. As a result, a significantly improved electrochemical performance has been attained for LRCF3, exhibiting enhanced capacity retention and reduced voltage fade (Fig. 3c).

In summary, we have proposed a facile ball-milling and electrochemical conversion strategy to realize *in situ* construction of a carbon and LiF-rich CEI coated on LRMO cathode. The dense coating layer significantly improves the surface stability of LRMO by preventing direct contact between the cathode surface and the electrolyte, thereby reducing side reactions and oxygen release. In addition, the production of carbon through electrochemical lithiation of CF can enhance the surface electronic conductivity of LRMO, resulting in outstanding rate and cycle performance. Furthermore, the moderate LiF-rich species with stable Li–F bonds can improve the electrochemical oxidation stability of the LRMO cathode, which slows down oxygen loss and irreversible phase transitions, leading to high capacity and enhanced cycling performance. Consequently, the synthesized LR@CF (3 wt% CF) demonstrates superior electrochemical performance with a high discharge capacity of 305.5 mA h g^{-1} (0.1C) and an improved ICE of 94.15%. Even at 5C, it still can deliver a discharge capacity of 213.1 mA h g^{-1}. Moreover, it also processes greatly enhanced capacity retention of 94.07% after 100 cycles at 1C. Our work provides an effective strategy for optimizing the electrochemical performance of LRMO materials, which could contribute to advancing the practical application.

This work is supported by the National Key R&D Program of China (2021YFB2500300), and the National Natural Science Foundation of China (Grant No. 52325207 and 22005333), and the New Energy Vehicle Power Battery Life Cycle Testing and Verification Public Service Platform Project (grant number 2022-235-224).

Data availability

The data supporting this article have been included as part of the ESI.†

Conflicts of interest

There are no conflicts to declare.

Notes and references

1 S. Xin, X. Zhang, L. Wang, H. Yu, X. Chang, Y.-M. Zhao, Q. Meng, P. Xu, C.-Z. Zhao, J. Chen, H. Lu, X. Kong, J. Wang, K. Chen, G. Huang, X. Zhang, Y. Su, Y. Xiao, S.-L. Chou, S. Zhang, Z. Guo, A. Du, G. Cui, G. Yang, Q. Zhao, L. Dong, D. Zhou, F. Kang, H. Hong, C. Zhi, Z. Yuan, X. Li, Y. Mo, Y. Zhu, D. Yu, X. Lei, J. Zhao, J. Wang, D. Su, Y.-G. Guo, Q. Zhang, J. Chen and L.-J. Wan, *Sci. China: Chem.*, 2024, **67**, 13–42.
2 Z. Yang, Y. Dai, S. Wang and J. Yu, *J. Mater. Chem. A*, 2016, **4**, 18210–18222.
3 G. Xu, Z. Liu, C. Zhang, G. Cui and L. Chen, *J. Mater. Chem. A*, 2015, **3**, 4092–4123.
4 B. Li and D. Xia, *Adv. Mater.*, 2017, **29**, 1701054.
5 Q. Li, Y. Yang, X. Yu and H. Li, *Chin. Phys. Lett.*, 2023, **40**, 048201.
6 W. Cao, Q. Li, X. Yu and H. Li, *eScience*, 2022, **2**, 47–78.
7 M. Chen, Y. Liu, Y. Zhang, G. Xing and Y. Tang, *Chem. Commun.*, 2022, **58**, 3591–3600.
8 X. Zhang, B. Wang, S. Zhao, H. Li and H. Yu, *eTransportation*, 2021, **8**, 100118.
9 C. S. Johnson, J.-S. Kim, C. Lefief, N. Li, J. T. Vaughey and M. M. Thackeray, *Electrochem. Commun.*, 2004, **6**, 1085–1091.
10 J.-J. Marie, R. A. House, G. J. Rees, A. W. Robertson, M. Jenkins, J. Chen, S. Agrestini, M. Garcia-Fernandez, K.-J. Zhou and P. G. Bruce, *Nat. Mater.*, 2024, **23**, 818–825.
11 W. Hua, X. Yang, N. P. M. Casati, L. Liu, S. Wang, V. Baran, M. Knapp, H. Ehrenberg and S. Indris, *eScience*, 2022, **2**, 183–191.
12 E. Hu, X. Yu, R. Lin, X. Bi, J. Lu, S. Bak, K.-W. Nam, H. L. Xin, C. Jaye, D. A. Fischer, K. Amine and X.-Q. Yang, *Nat. Energy*, 2018, **3**, 690–698.
13 X. Li, Y. Zhang, B. Qiu, G. Chen, Y. Zhou, Q. Gu and Z. Liu, *Energy Environ. Mater.*, 2024, **7**, e12722.
14 W. Zuo, M. Luo, X. Liu, J. Wu, H. Liu, J. Li, M. Winter, R. Fu, W. Yang and Y. Yang, *Energy Environ. Sci.*, 2020, **13**, 4450–4497.
15 W. He, W. Guo, H. Wu, L. Lin, Q. Liu, X. Han, Q. Xie, P. Liu, H. Zheng, L. Wang, X. Yu and D.-L. Peng, *Adv. Mater.*, 2021, **33**, 2005937.
16 B. Wang, Z. Zhuo, H. Li, S. Liu, S. Zhao, X. Zhang, J. Liu, D. Xiao, W. Yang and H. Yu, *Adv. Mater.*, 2023, **35**, 2207904.
17 Z. Zhu, R. Gao, I. Waluyo, Y. Dong, A. Hunt, J. Lee and J. Li, *Adv. Energy Mater.*, 2020, **10**, 2001120.
18 L. Di, C. Yufang, S. Weiwei, X. Wei, Y. Shuaiyu, L. Shiqiang, Z. Lanlan, Z. Yanshuang, Y. Tianyan, X. Peitao and Z. Chunman, *Adv. Energy Mater.*, 2023, **13**, 2301765.
19 Y. Pei, Q. Chen, Y. Ha, D. Su, H. Zhou, S. Li, Z. Yao, L. Ma, K. J. Sanders, C. Sheng, G. R. Goward, L. Gu, A. Yu, W. Yang and Z. Chen, *Angew. Chem., Int. Ed.*, 2022, **61**, e202212471.
20 Y. Wang, Z. Wu, F. M. Azad, Y. Zhu, L. Wang, C. J. Hawker, A. K. Whittaker, M. Forsyth and C. Zhang, *Nat. Rev. Mater.*, 2024, **9**, 119–133.
21 H. Wang, J. Liu, J. He, S. Qi, M. Wu, F. Li, J. Huang, Y. Huang and J. Ma, *eScience*, 2022, **2**, 557–565.
22 L.-B. Huang, L. Zhao, Z.-F. Ma, X. Zhang, X.-S. Zhang, Z.-Y. Lu, G. Li, X.-X. Luo, R. Wen, S. Xin, Q. Meng and Y.-G. Guo, *Angew. Chem., Int. Ed.*, 2024, e202413600.
23 Y. Yang, P. Li, N. Wang, Z. Fang, C. Wang, X. Dong and Y. Xia, *Chem. Commun.*, 2020, **56**, 9640–9643.
24 J. Moon, D. O. Kim, L. Bekaert, M. Song, J. Chung, D. Lee, A. Hubin and J. Lim, *Nat. Commun.*, 2022, **13**, 4538.
25 F. Zheng, Q. Deng, W. Zhong, X. Ou, Q. Pan, Y. Liu, X. Xiong, C. Yang, Y. Chen and M. Liu, *ACS Sustainable Chem. Eng.*, 2018, **6**, 16399–16411.
26 Y.-H. Tan, Z. Liu, J.-H. Zheng, Z.-J. Ju, X.-Y. He, W. Hao, Y.-C. Wu, W.-S. Xu, H.-J. Zhang, G.-Q. Li, L.-S. Zhou, F. Zhou, X. Tao, H.-B. Yao and Z. Liang, *Adv. Mater.*, 2024, **36**, 2404815.
27 C. Sun, Y. Feng, Y. Li, C. Qin, Q. Zhang and W. Feng, *Nanoscale*, 2014, **6**, 2634–2641.
28 A. Boulineau, L. Croguennec, C. Delmas and F. Weill, *Chem. Mater.*, 2009, **21**, 4216–4222.
29 Y. Yang, Y. Wang, Z. Xue, L. Zhang, L. Yan, Y. Luo and J. Xie, *J. Materiomics*, 2021, **7**, 585–592.
30 Y. Zhang, C. Yin, B. Qiu, G. Chen, Y. Shang and Z. Liu, *Energy Storage Mater.*, 2022, **53**, 763–773.
31 J. Zhou, Q. Chang, D. Zhang, L. Gao, Y. Gao, L. Wang, J. Shang and Y. Cao, *Appl. Surf. Sci.*, 2025, **679**, 161220.
32 J. Zhou, J. Chen, M. Chen, J. Wang, X. Liu, B. Wei, Z. Wang, J. Li, L. Gu, Q. Zhang, H. Wang and L. Guo, *Adv. Mater.*, 2019, **31**, 1807874.
33 Z. Lu, D. Liu, K. Dai, K. Liu, C. Jing, W. He, W. Wang, C. Zhang and W. Wei, *Energy Storage Mater.*, 2023, **57**, 316–325.